

1 **The Scanning Ion Conductance Microscope (SICM) for Cellular Physiology**

2 Max J Lab, Anamika Bhargava, Peter T Wright and Julia Gorelik*

3

4 Imperial College London, National Heart & Lung Institute,
5 Imperial Centre for Experimental and Translational Medicine,
6 Hammersmith Campus,
7 Du Cane Road,
8 London W12 0NN, UK.

9

10 **Running Head:** SICM for Cellular Physiology

11

12 *Corresponding author

13

14 Dr. Julia Gorelik
15 Imperial College London
16 National Heart and Lung Institute
17 4th floor, Imperial Centre for Translational and Experimental Medicine
18 Hammersmith Campus
19 Du Cane Road
20 London W12 0NN, UK
21 Tel 44(0)2075942736
22 Fax 44 020 7594 3653
23 E-mail: j.gorelik@imperial.ac.uk

24

25 Abstract

26 The quest for non-optical imaging methods that can surmount light diffraction limits
27 resulted in the development of Scanning probe microscopes, however most of
28 existing methods are not quite suitable for studying biological samples. The
29 scanning ion conductance microscope (SICM) bridges the gap between the
30 resolution capabilities of atomic force microscope and scanning electron microscope
31 and functional capabilities of conventional light microscope. A nanopipette mounted
32 on a three-axis piezo-actuator, scans a sample of interest and ion current is
33 measured between the pipette tip and the sample. The feedback control system
34 always keeps a certain distance between the sample and the pipette so the pipette
35 never touches the sample. At the same time pipette movement is recorded and this
36 generates a 3D topographical image of the sample surface. SICM represents an
37 alternative to conventional high-resolution microscopy, especially in imaging
38 topography of live biological samples. In addition the nanopipette probe provides a
39 host of added modalities, for example using the same pipette and feedback control
40 for efficient approach and seal with the cell membrane for ion channel recording.
41 SICM can be combined in one instrument with optical and fluorescent methods and
42 allows drawing structure-function correlations. It can also be used for precise
43 mechanical force measurements as well as vehicle to apply pressure with precision.
44 This can be done on living cells and tissues for prolonged periods of time without
45 them losing viability. The SICM is a multifunctional instrument, and it is maturing
46 rapidly and will open even more possibilities in the near future.

47

48 Keywords:

49 Cardiomyocytes, Cell mechanics, FRET, Smart patch-clamp, Topography, SICM

50

51 **Introduction**

52 The resolution of conventional microscopy has light diffraction limits (Table 1).
53 Electron microscopy surmounts this wavelength limit (15, 78), as does the non-
54 optical Scanning Probe Microscope (SPM). It does this by using nanoprobes (20, 46,
55 52, 83, 92, 115). The probe, mounted on a three-axis actuator platform scans a
56 sample of interest in the X and Y dimensions and together with recording of
57 displacement in the Z dimension generates a 3D image. Binnig and Rohrer scanned
58 the first samples using the Scanning Tunnelling Microscope (STM) in 1982, for
59 which they received the Nobel Prize. Electrons 'tunnel' between the surface of
60 interest and a very sharp stylus formed by a single atom enabling the mapping of
61 surface topography. Placing biological samples on a conductive base, the STM went
62 on to image their surfaces at very high resolutions (3). More recently, the self-
63 assembly of subunits of proteins (amino acids and peptides) was studied using STM
64 (121). The STM was the predecessor of other Surface Probe Microscopes, including
65 the prevalent atomic force microscope (AFM) (7) (Table 1). The AFM uses a sharp
66 tip mounted on a flexible cantilever, and the tip-sample interactions during scanning
67 deflect the tip which produces very high resolution images. This technology has
68 developed over time (1) and using an oscillating cantilever tip, has imaged large
69 molecules (94) including DNA (9). Due to the ability of AFM to image non
70 conducting surfaces, it has been widely used in biology to study cellular
71 macromolecules like protein-nucleic acid complexes, chromosomes, cellular
72 membranes and microbes. Recently, it has also been used for determining the
73 mechanical properties of skinned myocardial cells (126). The technique of
74 nanoindentation, traditionally performed via dedicated indenters can now be
75 reliably achieved using AFM instrumentation, enabling mechanical property
76 determination at the nanoscale. AFM nanoindentation capabilities have provided an

77 excellent improvement over conventional nanomechanical tools and by integration
78 of topographical data from imaging, enabled the rapid extraction and presentation
79 of mechanical data for biological samples (1). For example Jacot et al (50)
80 measured the elastic modulus of the epicardium using atomic force microscope
81 indentation and found that it significantly changes at birth, from an embryonic
82 value of 12 ± 4 kPa to a neonatal value of 39 ± 7 kPa. This change is in the range
83 shown to significantly affect the development of neonatal cardiomyocytes.

84 Biological cell surfaces commonly have a complex 3D nano-structure associated
85 with complex and dynamic function. The AFM's intermittent contact imaging mode
86 or 'tapping mode' circumvents these problems somewhat, and has been used for
87 imaging of biological cells and molecules (2, 13, 14, 27, 71, 87, 95, 108).

88 However, the use of force in AFM can be problematic in studying biological samples.
89 The cantilever tips can distort the image (123). Consequently this is an invasive
90 technique albeit at the nanometre scale. However, reducing the force reduces
91 surface indentation and improves its resolution, to reveal complex subcellular
92 structures such as microvilli (69). The other major method of probing biological
93 surfaces is scanning electron microscope (SEM), but it can only indirectly study
94 remnants of cell behaviour after the cells have been fixed (frozen) (41, 76).

95 By contrast, optical methods, and in particular fluorescent microscopy, are more
96 suited to study functionality by localizing fluorescently labelled molecules within the
97 cell. But this does not directly image cell surfaces (74, 119), neither can it reach
98 the resolution of the above two methods (Table 1). However, the Scanning Ion
99 Conductance Microscope (SICM) bridges the gap between the resolution capabilities
100 of AFM / SEM, and functional capabilities of conventional light microscopy (Table 1).

101

102

103 **1. Principle of SICM Operation**

104 Scanning Ion Conductance Microscopy is a relatively new technique, first used by
105 Paul Hansma in 1989 (40). Its development was continued by Yuri Korchev starting
106 in 1997 (35, 55, 57-61). In this microscope a sharp borosilicate glass nanopipette
107 (with the inner diameter below 200 nm) is used as a probe.

108 The pipette can move during the scan, or as in Figure 1, the sample moves, being
109 similarly mounted on the XY piezo. In this case, the pipette does not move laterally,
110 just vertically (Z). To start, the pipette approaches the sample progressively
111 decreasing the pipette-sample distance. This gradually restricts ions flowing
112 through the fluid-filled pipette thus decreasing the current. The ion current through
113 the pipette depends on the overall resistance of the tip, which is the combination of
114 the resistance of the micropipette itself and the access resistance of the
115 micropipette opening. Access resistance is a complex function of the distance
116 between the sample and the probe, and the geometry and electrochemical
117 properties of the sample surface. This current (I) through the pipette, which is
118 measured directly, is given by:

$$119 \quad I = V/R_p + R_a(d)$$

120 Where V = voltage applied to the electrode, R_p = pipette resistance, R_a = access
121 resistance and d = distance between sample and the probe.

122 A distance-modulated feedback control system keeps the ionic conductance and
123 thus the sample/pipette distance constant. Typically the feedback control stops the
124 approach at a pre-defined distance or "set point". With the feedback loop controlling
125 ion conductance the pipette never touches the sample – it stops at a distance
126 equivalent to the inner radius of the pipette. This enables non-contact scanning. As
127 the scan proceeds in the X and Y directions the ion conductance control system

128 detects changes in nanopipette displacement in the Z direction. These recorded
129 signals build up a computerised 3D image of the sample surface (Figure 1).

130 The pipette's inner tip diameter is typically 20-100 nm. As the resolution depends
131 upon the radius of the pipette inner tip (97), the SICM can obtain a resolution of 10
132 nm with a tip size of 20 nm diameter. The limitation of the tip size is around 10-12
133 nm.

134 In order to scan living cells, we require displacements in excess of 50 μm .
135 Therefore, the SICM uses a 3 axis piezo translation stage (Jena, Germany) with 100
136 μm travel distance in X Y and Z directions. This can image an area of 100 x 100 μm
137 in a single scan. The lateral image resolution is usually 512x 512 pixels. A single
138 scan can take several minutes depending on the resolution at which it is being
139 acquired, and the area scanned. For example a 10 x 10 μm scan of an isolated
140 adult cardiomyocyte with 150 nm resolution takes between 2-3 minutes. Although
141 the SICM's resolution is not as high as that of the AFM, SICM is potentially an
142 alternative to conventional high-resolution microscopy technologies, especially in
143 the imaging of live biological samples (e.g. Figure 2). Importantly, the pipette probe
144 provides a remarkable set of added capabilities (55, 107, 112). As described below,
145 this multi-functionality makes the SICM a platform for the convergence of different
146 microscopic and investigative technologies.

147 **2. Typical hardware of SICM**

148 A typical SICM uses an inverted microscope (e.g. Diaphot 200 or TE200; Nikon
149 Corporation, Tokyo, Japan). Sample positioning is achieved by a computer-
150 controlled piezotranslation stage mounted on the microscope stage (ICnano sample
151 scan system -Ionscope Ltd, UK) with 100 x 100 μm x-y piezo-actuator for sample
152 movement and a 25 μm z-axis piezo-actuator for pipette movement. The piezo

153 stage holds the glass nanopipette, which is connected to the head-stage of the
154 feedback amplifier (Figure 1).

155 The SICM can use either a resistive or capacitive feedback head-stage like Axopatch
156 200B or Multiclamp 700B (Molecular devices Sunnyvale, CA). Ag/AgCl electrodes, in
157 the bath and pipette, provide electrical connection as in a conventional
158 electrophysiological circuit. Additional electronic components include a digitizer and
159 computer controlled software. The SICM has stringent requirements to cope with
160 vibration and electrical noise - particularly for "smart patch-clamp." The SICM setup
161 rests on a vibration isolation table commonly used in electrophysiology. A small
162 faraday cage on the microscope stage encloses the piezo axis translation stage, for
163 electrical isolation and minimising noise.

164 **3. "Hopping Probe" Scanning Ion Conductance Microscope (HPSICM)**

165 Tall structures on the surface of biological cells can pose problems in lateral
166 scanning. The pipette tip may collide with and drag the structures producing image
167 artefacts, or the tip can break. To overcome this, Pavel Novak and colleagues
168 developed the "hopping" mode of the SICM (HPSICM) as a modification of the
169 scanning procedure (86). In a system with this modification, the pipette "hops" as it
170 scans and it no longer needs continuous feedback to keep a fixed sample-probe
171 distance. The pipette starts well above a surface feature, producing a maximal
172 current at this starting distance from the surface. From this point the pipette
173 approaches, reducing the ion current to a pre-defined 0.25-1%. The height of the
174 sample at this imaging point is the recorded Z-position. With the ion current
175 reduced by 1%, the tip is still at a one inner pipette radius from the surface and still
176 avoids cell surface contact. The pipette withdraws and then the sample moves
177 laterally to the next imaging point. Importantly, by updating the maximal current
178 continuously while the pipette is withdrawn from the surface, the system

179 automatically compensates for slow drift in pipette current. HPSICM also minimises
180 image-distorting noise as the pipette spends most of its time away from the image
181 sampling point of interest. A direct comparison between images of soft biological
182 samples obtained with the AFM and SICM showed that the SICM images were better
183 than AFM which distorts the image (96).

184 **4. Imaging of cell surface topography.**

185 The SICM has produced 3D topographical images of cells that are unfixed,
186 unstained, and alive, with resolutions approaching that of AFM and electron
187 microscopes (96, 106). For SICM imaging, living cell samples need no fixing or
188 mounting. Cells are placed in petridishes or on the coverslips on which they were
189 grown. In the latter case, for purely topographical studies the cells are bathed in
190 growth media, which is also used to fill the pipette. In other studies, for example
191 "smart" patch-clamp, the external (bath solution) and internal (pipette solution) are
192 determined by the requirements of the electrophysiological study (e.g. ion channel
193 studies (35)).

194 Images of mouse ear hair cells were produced using SICM which have a true
195 fidelity, as demonstrated when comparing them with images produced with a
196 scanning electron microscope after cells were fixed and shaded. Surface
197 topographical images of cardiomyocytes show complex structures with grooves
198 related to the Z disc, with invaginations that represent T-tubule openings (Figure 2A
199 & C). One can calculate the average length of Z-grooves on the surface of the
200 myocytes to produce a measurement of the surface structure regularity. This
201 indicator has proven to be valuable in following surface structural changes in
202 cardiomyocytes that occur during heart failure (72). SICM cardiovascular imaging
203 has not been confined to myocardial cells and for example images of aortic and
204 heart valve endothelium have been obtained. Endothelial cells from aorta were

205 cultured in transwell plates under static conditions or on an orbital shaker that
206 generated shear stress. In static conditions endothelial cells oriented randomly but
207 when shear stress was applied they became aligned (93). In another study the
208 fragments of living aortic tissues were examined. Endothelium from the outer curve
209 of aorta showed orientation along the direction of blood flow, whereas the inner
210 curve showed no orientation. This has been demonstrated in the past with other
211 microscopy techniques but SICM resolves this physical alignment in living tissue.
212 Also SICM has been applied to study the differences between membrane
213 compliance in these cells (93).

214 **5. Structure-Function Correlation.**

215 Compartmentalization of calcium (5, 43, 89) and other second messengers (12, 47,
216 63) is crucial to cellular function. The plasma membrane is rich in receptors and ion
217 channels that respond to corresponding ligands by generating second messengers
218 in signaling microdomains. For example G-Protein Coupled Receptors can change
219 their signaling properties depending on their cellular locations (11, 120). Protein
220 kinases and phosphatases can also form structurally determined microdomains by
221 specific localization to the cytoskeleton thus facilitating heterogeneous
222 compartmentation (102). The AFM has been used to localize membrane receptors in
223 cardiac tissue by combining fluorescence imaging and topography (23), but the
224 SICM expands this type of use, which we will describe in the following section.

225 **6.1. Localized beta adrenergic receptor-dependent cAMP signaling.**

226 Combining SICM with Foster Resonance Energy Transfer (FRET) technique allowed
227 Nikolaev et al to follow nano-scale signaling changes in defined sub-cellular regions,
228 in living cardiomyocytes (Figure 2) (85). The SICM resolved T-tubules openings on
229 the membrane of cardiomyocytes (Figure 2C) expressing a FRET sensor (EPAC2-
230 camps) for the second messenger cAMP. When selectively stimulating beta-2

231 receptors (β_2 AR), cAMP was only produced when applying its agonist selectively
232 above a T-tubule, and the resultant cAMP signal was spatially confined (Figure 2D).
233 This provides a degree of control for the β_2 AR signaling mechanism - A situation in
234 contrast to the beta-1 receptor (β_1 AR) signaling, which is not spatially confined and
235 is present equally in all membrane regions. In failing cardiomyocytes (Figure 2E),
236 β_2 AR signal was no longer constrained to the T-tubules (Figure 2F), which may be a
237 contributory factor in the pathology of heart failure. They redistributed from the T
238 tubules to the crests. This alters cyclic-AMP signal compartments with possible
239 pathophysiological consequences.

240 This hybrid SICM/FRET technique may be an important avenue in studying other
241 localized receptors. Moreover, as well as responses to pharmacological stimuli,
242 SICM/FRET could investigate molecular mechanosensitivity. Recent studies by the
243 Schwartz group (33) used a FRET sensor based on vinculin to resolve piconewton
244 stresses on vinculin in focal adhesions. We could envisage a possible future
245 development of SICM/FRET in this direction. By applying pressure via the SICM
246 pipette a combination of SICM and a FRET sensor could investigate these dynamic
247 processes. It could also investigate cellular networks and contacts to monitor the
248 effects of stimulating single cells in a network, of adherent cells.

249 **6.2 Mapping ion channels with an added patch system.**

250 The SICM has been combined with a conventional whole-cell patch-clamp setup. In
251 this combination, the SICM non-contact scan can provide a map of the location of
252 KATP channels (60). In this setup current images were recorded over some 40 min
253 and showed low lateral mobility of KATP channels, but they concentrate in
254 sarcolemmal Z grooves. The SICM pipette with K^+ inside, applied K^+ while scanning
255 the cell surface. A second patch-clamp pipette in the whole-cell mode records patch
256 currents as the SICM probe scans over and activates a KATP channel. This

257 information can be related to the position of the SICM probe to create a distribution
258 map of KATP channels, or with appropriate activation and markers, other particular
259 ion channels.

260 **6.3 Mapping Ion Channels with SICM as the Patch-Clamp System (The** 261 **“Smart Patch-Clamp” technique)**

262 The mapping of ion channels has been facilitated by using the same pipette both to
263 image the surface of a cardiomyocyte and to function as the electrophysiological
264 probe. In this technique, a high resistance glass nanopipette first scans the cell
265 surface to produce a high-resolution topographic image of the cell surface. The
266 topographic image is used to precisely position the pipette onto a cellular
267 nanodomain of choice (we have the XY coordinates.) The same glass nanopipette is
268 then used to obtain single ion channel currents using the patch-clamp technique. In
269 the conventional patch-clamp technique the pipette approaches the target manually
270 and often obliquely to visualise the pipette tip placement through the microscope.
271 By contrast, pipette-approach with the SICM is vertical, almost fully automatic, and
272 precisely controlled by the distance modulated feedback system. At a
273 predetermined distance from the precisely selected target location the feedback
274 control is switched off to allow a controlled contact with the membrane. The
275 frequency of successful patches is significantly higher with this approach than with
276 the conventional method (31). SICM distance-modulated feedback control is useful
277 as the glass pipette will not touch the cell until required, and damage to the cell or
278 pipette is minimised. As a result, “smart” patch-clamp technique records ion
279 channel activity from precise nanodomains on the surface of live cells and thus can
280 generate a spatial functional map of surface ion channels. This is in contrast to
281 conventional patch-clamping where the position of the pipette with respect to the
282 cell topography cannot be controlled with a nanoscale precision. The method is also

283 superior to the current conventional microscopic techniques (immunofluorescence)
284 which target all the channels including the dormant ones, whereas the "smart"
285 patch-clamp technique locates only the functional ion channels.

286 Yuri Korchev and co-workers developed and successfully applied the "smart" patch-
287 clamp to record ion channels from several different cell types (31, 35). Ion currents
288 were recorded from very small cells (e.g. sea urchin sperm cells) and fine focal
289 swellings (boutons) in neuronal processes of 0.5-1.0 μm in diameter, which
290 otherwise would have been extremely difficult to patch. That is, it can successfully
291 record from membrane structures that are too small to be resolved conventionally
292 or that cannot be detected by light microscopy e.g. from T-tubules of
293 cardiomyocytes. The "Smart" patch-clamp system produced a spatial map of L-type
294 calcium channels on a cardiomyocyte surface (setup shown in Figure 3B). Figure 3A
295 shows the optical image of an isolated cardiomyocyte and position of the
296 nanopipette. Figure 3C shows a 10 μm x 10 μm topography scan of the same
297 cardiomyocyte. "Smart" patch-clamp at different locations (e.g. T-tubules, crest or
298 groove, Figure 3D) provided the first direct evidence of functional ion channel
299 location. A representative L-type calcium channel activity from a T-tubule is shown
300 in Figure 3E. The study showed a preferential location of L-type calcium channels to
301 the T-tubules (Figure 3F) where they are in close proximity to other proteins
302 involved in excitation-contraction coupling (6, 88).

303 The "Smart" patch-clamp also recorded ion channel currents from opaque samples
304 (e.g. aorta, brain slices, and cells grown on filters). Optically guided patch-clamp
305 prevents the collection of any information on the position or type of cellular
306 structure. In another study, Gu and co-workers mapped not only calcium channels
307 but also chloride channels on the surface of cardiomyocytes and found that these
308 are not randomly distributed but have a specific location on cardiomyocyte

309 membrane (three Cl⁻ channels are located only in z grooves and T-tubule
310 openings) where they may have synergistic roles in excitation-contraction coupling
311 (35).

312 A. K. Dutta and co-workers used smart-patch to record maxi-anion channels from
313 cardiomyocytes which could not be recorded using conventional patch-clamp (24).
314 The advantage of "smart" patch-clamp here would be to visualize structures where
315 the ion channels could be clustered which could easily be missed in conventional
316 patch-clamp.

317 **6. Tracking Dynamic Biological Processes**

318 **7.1 Dynamics of membrane structures.**

319 Unlike the other high resolution microscopes, the fact that the SICM can scan live
320 cells in real time means it can follow biological processes taking place at cell
321 membrane surfaces (125) including large membrane proteins (104, 106). In the
322 high resolution mode the SICM can scan an area of 1 μm square in 9 seconds per
323 frame. This can follow the appearance and disappearance of microvilli and the
324 opening and closing of endocytotic pits. With the improved topographical resolution,
325 Shevchuk et al (105) found that the SICM can visualize the opening and closing of
326 clathrin pits, which are $\sim 200\text{-nm}$ indentations in the membrane. It appears that
327 most pits close with the help of a membrane protrusion that forms beside the pit.
328 After simultaneous confocal detection of fluorescence in cells expressing GFP-
329 labelled proteins they found that clathrin, dynamin and several other actin-binding
330 proteins, for example Flotillin 1 and 2 co-localize with pits when these undergo
331 morphological changes.

332 The SICM has revealed movements and reorganization of microvilli in real time on
333 the surface of different types of epithelial cells (32). Microvilli appear and grow at a
334 rate of about 5 nm/s over 2 and a half minutes, and after reaching a plateau lasting

335 some 5 minutes and retract at about 1.2 nm/s. Moreover, they tend to form
336 migrating clusters.

337 **7.2 Cell Volume Measurements**

338 Cell volumes can dynamically change. Osmotic changes following early myocardial
339 ischemia and cell changes in myocardial hypertrophy require complex cell-shape
340 and volume reorganization (38, 45). Several indirect techniques (16, 53) and some
341 more direct methods(84) have been used to measure and monitor cell volume. The
342 latter method is only applicable to cells of nearly spherical shape and in suspension.
343 Light microscopy methods have also been used (26, 75). An advanced method for
344 cell volume measurement uses scanning laser confocal microscopy (25, 36, 127).
345 However, generally, these methods have limited spatial resolution, and the cell
346 plasma membrane cannot always be clearly visualized. The SICM can measure cell
347 volumes between 10^{-19} and 10^{-9} litre (58) The SICM measures volume by integrating
348 the raster image (Z-displacement) in X and Y directions, of the whole cell assuming
349 that the entire cell's basal surface is in close contact with the substrate (58). As a
350 reference, we measure the Z position of the pipette touching the substrate. This
351 technique can also measure smaller volumes such as in lamellopodia, dendritic
352 processes, or microvilli, with 2.5×10^{-20} liter resolution.

353 **7. SICM as a Non-Invasive Mechanical (Distance and Force) Probe**

354 **8.1 Contraction**

355 Hovering over a contracting myocyte the SICM distance feedback control can follow
356 and record Z-displacement of the nanopipette and therefore record the event of
357 contraction as an upwards membrane movement. Figure 4A diagrams the system
358 for recording contraction and monitoring calcium transients. The system records
359 and digitizes the Z piezo position which follows the physical contraction of the
360 membrane (Figure 4B – black trace)

361 **8.2 Cell membrane compliance**

362 Cellular mechanical properties are determined by its intracellular mechanical
363 characteristics such as cell structures, molecules, and downstream signals
364 associated with the cytoskeleton (51). On the other hand, mechanical properties of
365 the cell membrane contribute to cellular function (90). Being heterogeneously
366 supported by the cytoskeleton, membrane varies its mechanical properties at the
367 nanoscale. It is important to use adequate mechanical investigative tools while
368 studying cells that are alive and with soft surfaces.

369 Different methods have been applied to study membrane compliance, e.g.
370 micropipette aspiration (44) and optical tweezers (17, 111). The AFM's cantilever
371 can measure forces at the molecular level (73, 113, 114, 124), and it has also
372 proved to be suitable for mapping local mechanical properties at nano-scales (21,
373 22, 37, 42, 68, 99, 103, 109) and relate this to cell topography. It has shown
374 heterogeneity of micromechanical properties of cultured atrial myocytes, which
375 correlated with cytoskeletal structure (fluorescence imaging). Pressing the AFM's
376 cantilever on to cell surfaces has studied cell compliance and elasticity (2, 28, 64,
377 117).

378 But as described above, the AFM's cantilever directly and undesirably contacts the
379 cell surface. Any use of force in these soft cell membranes will compromise
380 attempts at determining any heterogeneity in the cell's mechanical properties. The
381 SICM based system overcomes some of these difficulties (100), and its distance
382 control may be employed to probe cell mechanics. A pressure source down the
383 nanopipette generates force at the tip. This force is calibrated, using the AFM
384 cantilever as the gold standard, with applied pipette pressure bending the
385 cantilever. The SICM distance feedback control ensures the pipette follows the

386 bending lever. Pipette pressure is converted to force (100) and the pressure applied
387 at the pressure port is developed at the pipette tip.

388 Using hydraulic jets applied to indent surface membranes, the SICM has studied the
389 mechanical properties of some cell types (100).

390 We (100) initially calibrated the SICM using an AFM cantilever with a spring
391 constant of 0.01 N/m. Pipette pressure on the cantilever bends the lever, and we
392 can measure the corresponding change in pipette position. Control experiments
393 over a glass coverslip showed no detectable change in pipette position with applied
394 hydrostatic pressure indicating that this does not alter the ion current. The
395 relationship between the cantilever deformation and applied pressure was linear,
396 with no hysteresis. This was also observed using pipettes of different resistance and
397 hence inner radius. Since we know the spring constant of the cantilever, the
398 distance moved by the cantilever can be directly converted into force using $F = k$
399 (spring constant) \times (distance) allowing a direct conversion of applied pressure into
400 applied force. The force exerted on the cantilever should also depend on the applied
401 pressure and pipette radius. The pipette radius, R_0 , can be calculated from the
402 pipette resistance (R_p) using

403
$$R_p = 1 / (\pi \xi R_0 \tan \theta)$$

404 Where θ is the half cone angle of the inner wall of the pipette (1.5 degrees in our
405 case) and ξ is the conductance of the solution. This formula was verified
406 experimentally using scanning electron microscopy or optical microscopy of pipettes
407 of measured resistance to directly determine R_0 . We then obtained a plot of the
408 force exerted on the cantilever per kPa, for pipettes of different resistances.

409

410 Specifically, SICM has been used to explore the mechanical properties of
411 cardiomyocytes with their characteristic repetitive scalloped topographic features.

412 The distance feedback control ensures that the pipette follows the indentation,
413 which is a function of the applied pressure. This quantitatively probes the cell
414 surface without direct contact. Knowing the effective force and distance one can
415 determine a Young's Modulus of Elasticity. A hydraulic jet produces an initial small
416 200 nm indentation (Young's Modulus 1.3 kPa) followed by a larger indentation,
417 with a larger Young's Modulus (2.8 kPa) (100). This component of the SICM not
418 only probes mechanical properties of cells, but can also map any nano-
419 heterogeneity in mechanical properties. A study in cardiomyocytes from heart
420 failure shows changes in surface topography - Z grooves and t tubules (72) and the
421 precise factors leading to this change are unclear.

422 **8.3 Nano-Mechanotransduction and Mechanosensitivity**

423 Mechanotransduction and mechanosensitivity is highly conserved and exists
424 throughout biology (79). It involves mechanosensitive ion channels (29, 80),
425 membrane and intracellular molecules, downstream intracellular signals and
426 intracellular structures, including the cytoskeleton. Cellular mechanosensitivity is a
427 burgeoning study area of rapidly increasing importance (39), particularly in heart
428 (4, 10, 49, 56, 66, 118), and the vasculature (34, 48, 54, 82). The SICM was first
429 used to study the mechanics of neurons (100) where a hydraulic jet could clearly
430 indent the membrane. However, in cardiac myocytes a hydraulic jet (system
431 diagrammed Figure 4C) can not only indent the membrane (Figure 4D -
432 subthreshold pressure, left hand block arrow), but this indentation reached a
433 threshold magnitude to activate contraction of the cardiomyocyte (65) (Figure 4D -
434 threshold pressure right hand block arrow). That is, a mechanically induced
435 potentially arrhythmogenic beat.

436 In an extended study (77) myocardial cells were loaded with Fluo-4 AM, a calcium
437 sensitive dye. The SICM pipette initially scanned the cell membrane, with no applied

438 pipette pressure, producing a 3D image of membrane topology. Then pipette
439 pressure is applied to selected coordinates, targeting crests, Z-grooves, or T-
440 tubules. The jets indent the membrane activating a mechanosensitive calcium
441 response, and these are determined by the cell's regional mechanical properties.
442 The calcium response remains highly localized when pressure is applied over a
443 groove, and spreads through the whole cell when the pressure is applied over a
444 crest. The SICM has revealed the normal regular repetitive surface topography (see
445 Figure 2A) of a myocardial cell, but cardiomyocytes from failing myocardium show
446 surface disruption with no regular striations (see Figure 2E) and strikingly, hydraulic
447 jets can generate an abnormal activating calcium signal regardless of the position
448 of applied pressure.

449 **8. General Perspectives and Conclusion**

450 The nanopipette platform lends itself to label-free biosensing, using specific
451 recognition compounds for analysis (19). For use in microinjection, it confers
452 advantages over conventional techniques, with superior control over delivery, and
453 the possible use of voltage instead of pressure to drive delivery. Thus more cells
454 survive injection (the force produced by applying voltage across the liquid/liquid
455 interface, which changes the surface tension, is enough to produce pipette flow). A
456 few studies have provided results with this technique (8, 67, 91, 110). The SICM is
457 not just a microscope as indicated in the left hand side of Figure 5. Because it uses
458 a nanopipette as its scanning probe, it is a multifunctional convergent instrument
459 (Figure 5 right hand side). It is a rapidly maturing technology. The potential of the
460 "smart" patch-clamp method is yet to be fully explored. It can potentially be used
461 to identify electrophysiological changes associated with morphological changes that
462 occur in different circumstances, e.g. with cell differentiation from precursor cells
463 (30). Moreover, combining "smart" patch-clamp and FRET-based signaling may

464 open new avenues of SICM application in cell physiology and pathology. An electron
465 microscopic estimate of populations of membrane channels showed that stereo
466 imaging is superior to non-stereo imaging for quantifying surface channels and
467 receptors (62). Electron microscopy can provide a means of counting receptors and
468 ion channels on freeze-fractured membranes. But because it uses freeze fracture,
469 the number of functional channels cannot be estimated. Improved SICM scanning
470 and electrophysiological procedures may provide accurate estimates of functional
471 channels with nanometre precision.

472 Also, delivery through the pipette using pressure and/or voltage opens a host of
473 possibilities (122). A multi-barrelled pipette can deliver multiple ligands such as
474 agonists/inhibitors (98, 112). The SICM nano-pipette may be turned into highly
475 sensitive electrochemical sensor, for spatiotemporal distribution of electrochemical
476 mediators. The amount of substance released at different pressures and voltages
477 can be calibrated and the release of chemicals from the pipette can be precisely
478 controlled. By this, the nano-pipette can concentrate and control chemicals at the
479 tip to trigger localized receptor mediated response opening the possibility of
480 functional mapping of receptor mediated responses in cardiomyocytes and other
481 biological cells. Local delivery enables replication in delivery of chemical agents to
482 the same cellular structures at multiple points in the same dish without exposing
483 neighbouring cells, or indeed other parts of the cell, to the drug. This could enable
484 rapid drug testing experiments effectively at the nano-level that has not been
485 possible previously.

486 The fact that the SICM uses a glass pipette for its probe, not only confers many
487 purely biological applications (55), it is also useful in mechanobiology. In the latter
488 case, force-based studies similar to that in the AFM (70), but noninvasively, will
489 show whether the stiffness (Young's Modulus of Elasticity) changes during

490 development, repair and regeneration, neoplasia, and heart pathology. Finally, the
491 pipette lends itself to sense probing, and nanofabrication.

492

493 **References**

- 494 1. **Allison DP, Mortensen NP, Sullivan CJ, and Doktycz MJ.** Atomic force
495 microscopy of biological samples. *WileyInterdiscipRevNanomedNanobiotechnol*
496 2: 618-634, 2010.
- 497 2. **Azeloglu EU, and Costa KD.** Atomic force microscopy in mechanobiology:
498 measuring microelastic heterogeneity of living cells. *Methods MolBiol* 736:
499 303-329, 2011.
- 500 3. **Baro AM, Miranda R, Alaman J, Garcia N, Binnig G, Rohrer H, Gerber C,**
501 **and Carrascosa JL.** Determination of surface topography of biological
502 specimens at high resolution by scanning tunnelling microscopy. *Nature* 315:
503 253-254, 1985.
- 504 4. **Baumgarten CM, Browe DM, and Ren Z.** Swelling- and Stretch-activated
505 Chloride Channels in the Heart: Regulation and Function. 2005.
- 506 5. **Berridge MJ.** Calcium microdomains: organization and function. *Cell Calcium*
507 40: 405-412, 2006.
- 508 6. **Bers DM.** Cardiac excitation-contraction coupling. *Nature* 415: 198-205,
509 2002.
- 510 7. **Binnig G, Quate CF, and Gerber C.** Atomic force microscope. *PhysRevLett*
511 56: 930-933, 1986.
- 512 8. **Bruckbauer A, Zhou D, Ying L, Korchev YE, Abell C, and Klenerman D.**
513 Multicomponent submicron features of biomolecules created by voltage
514 controlled deposition from a nanopipet. *JAmChemSoc* 125: 9834-9839, 2003.
- 515 9. **Bustamante C, Vesenka J, Tang CL, Rees W, Guthold M, and Keller R.**
516 Circular DNA molecules imaged in air by scanning force microscopy.
517 *Biochemistry* 31: 22-26, 1992.

- 518 10. **Calaghan SC, and White E.** Mechanical Modulation of Intracellular Ion
519 Concentrations: Mechanisms and Electrical Consequences. 2005.
- 520 11. **Calebiro D, Nikolaev VO, Persani L, and Lohse MJ.** Signaling by
521 internalized G-protein-coupled receptors. *Trends PharmacolSci* 31: 221-228,
522 2010.
- 523 12. **Cheuk W, and Chan JK.** Subcellular localization of immunohistochemical
524 signals: knowledge of the ultrastructural or biologic features of the antigens
525 helps predict the signal localization and proper interpretation of immunostains.
526 *IntJSurgPathol* 12: 185-206, 2004.
- 527 13. **Cho SJ, Wakade A, Pappas GD, and Jena BP.** New structure involved in
528 transient membrane fusion and exocytosis. *AnnNYAcadSci* 971: 254-256,
529 2002.
- 530 14. **Colton RJ, Baselt DR, Dufrene YF, Green JB, and Lee GU.** Scanning probe
531 microscopy. *CurrOpinChemBiol* 1: 370-377, 1997.
- 532 15. **Cong Y, and Ludtke SJ.** Single particle analysis at high resolution. *Methods*
533 *Enzymol* 482: 211-235, 2010.
- 534 16. **Crowe WE, Ehrenfeld J, Brochiero E, and Wills NK.** Apical membrane
535 sodium and chloride entry during osmotic swelling of renal (A6) epithelial cells.
536 *JMembrBiol* 144: 81-91, 1995.
- 537 17. **Dai J, and Sheetz MP.** Mechanical properties of neuronal growth cone
538 membranes studied by tether formation with laser optical tweezers. *BiophysJ*
539 68: 988-996, 1995.
- 540 18. **de Jonge N, Peckys DB, Kremers GJ, and Piston DW.** Electron microscopy
541 of whole cells in liquid with nanometer resolution. *Proceedings of the National*
542 *Academy of Sciences of the United States of America* 106: 2159-2164, 2009.

- 543 19. **Ding S, Gao C, and Gu LQ.** Capturing single molecules of immunoglobulin
544 and ricin with an aptamer-encoded glass nanopore. *AnalChem* 81: 6649-6655,
545 2009.
- 546 20. **Domke KF, and Pettinger B.** Studying surface chemistry beyond the
547 diffraction limit: 10 years of TERS. *Chemphyschem* 11: 1365-1373, 2010.
- 548 21. **Dufrene YF, Boonaert CJP, van der Mei HC, Busscher HJ, and Rouxhet**
549 **PG.** Probing molecular interactions and mechanical properties of microbial cell
550 surfaces by atomic force microscopy. *Ultramicroscopy* 86: 113-120, 2001.
- 551 22. **Dulinska I, Targosz M, Strojny W, Lekka M, Czuba P, Balwierz W, and**
552 **Szymonski M.** Stiffness of normal and pathological erythrocytes studied by
553 means of atomic force microscopy. *JBiochemBiophysMethods* 66: 1-11, 2006.
- 554 23. **Duman M, Pflieger M, Zhu R, Rankl C, Chtcheglova LA, Neundlinger I,**
555 **Bozna BL, Mayer B, Salio M, Shepherd D, Polzella P, Moertelmaier M,**
556 **Kada G, Ebner A, Dieudonne M, Schutz GJ, Cerundolo V, Kienberger F,**
557 **and Hinterdorfer P.** Improved localization of cellular membrane receptors
558 using combined fluorescence microscopy and simultaneous topography and
559 recognition imaging. *Nanotechnology* 21: 115504, 2010.
- 560 24. **Dutta AK, Korchev YE, Shevchuk AI, Hayashi S, Okada Y, and Sabirov**
561 **RZ.** Spatial distribution of maxi-anion channel on cardiomyocytes detected by
562 smart-patch technique. *BiophysJ* 94: 1646-1655, 2008.
- 563 25. **Errington RJ, Fricker MD, Wood JL, Hall AC, and White NS.** Four-
564 dimensional imaging of living chondrocytes in cartilage using confocal
565 microscopy: a pragmatic approach. *AmJPhysiol* 272: C1040-C1051, 1997.
- 566 26. **Farinas J, Kneen M, Moore M, and Verkman AS.** Plasma membrane water
567 permeability of cultured cells and epithelia measured by light microscopy with
568 spatial filtering. *JGenPhysiol* 110: 283-296, 1997.

- 569 27. **Francis LW, Lewis PD, Wright CJ, and Conlan RS.** Atomic force
570 microscopy comes of age. *BiolCell* 102: 133-143, 2010.
- 571 28. **Frederix PL, Bosshart PD, and Engel A.** Atomic force microscopy of
572 biological membranes. *BiophysJ* 96: 329-338, 2009.
- 573 29. **French AS.** Mechanotransduction. *Annual review of physiology* 54: 135-152,
574 1992.
- 575 30. **Gorelik J, Ali NN, Sheikh Abdul Kadir SH, Lab M, Stojkovic P,**
576 **Armstrong L, Sviderskaya EV, Negulyaev YA, Klenerman D, Bennett**
577 **DC, Lako M, Harding SE, Stojkovic M, and Korchev YE.** Non-invasive
578 imaging of stem cells by scanning ion conductance microscopy: future
579 perspective. *Tissue Eng Part CMethods* 14: 311-318, 2008.
- 580 31. **Gorelik J, Gu Y, Spohr HA, Shevchuk AI, Lab MJ, Harding SE, Edwards**
581 **CR, Whitaker M, Moss GW, Benton DC, Sanchez D, Darszon A,**
582 **Vodyanoy I, Klenerman D, and Korchev YE.** Ion channels in small cells
583 and subcellular structures can be studied with a smart patch-clamp system.
584 *BiophysJ* 83: 3296-3303, 2002.
- 585 32. **Gorelik J, Shevchuk AI, Frolenkov GI, Diakonov IA, Lab MJ, Kros CJ,**
586 **Richardson GP, Vodyanoy I, Edwards CR, Klenerman D, and Korchev**
587 **YE.** Dynamic assembly of surface structures in living cells.
588 *ProcNatlAcadSciUSA* 100: 5819-5822, 2003.
- 589 33. **Grashoff C, Hoffman BD, Brenner MD, Zhou R, Parsons M, Yang MT,**
590 **McLean MA, Sligar SG, Chen CS, Ha T, and Schwartz MA.** Measuring
591 mechanical tension across vinculin reveals regulation of focal adhesion
592 dynamics. *Nature* 466: 263-266, 2010.
- 593 34. **Groschner K.** Two ways to feel the pressure: an endothelial Ca(2+) entry
594 channel with dual mechanosensitivity. *CardiovascRes* 53: 9-11, 2002.

- 595 35. **Gu Y, Gorelik J, Spohr HA, Shevchuk A, Lab MJ, Harding SE, Vodyanoy**
596 **I, Klenerman D, and Korchev YE.** High-resolution scanning patch-clamp:
597 new insights into cell function. *FASEB J* 16: 748-750, 2002.
- 598 36. **Guilak F.** Volume and surface area measurement of viable chondrocytes in
599 situ using geometric modelling of serial confocal sections. *JMicrosc* 173: 245-
600 256, 1994.
- 601 37. **Haga H, Sasaki S, Kawabata K, Ito E, Ushiki T, and Sambongi T.**
602 Elasticity mapping of living fibroblasts by AFM and immunofluorescence
603 observation of the cytoskeleton. *Ultramicroscopy* 82: 253-258, 2000.
- 604 38. **Hallows KR, Law FY, Packman CH, and Knauf PA.** Changes in cytoskeletal
605 actin content, F-actin distribution, and surface morphology during HL-60 cell
606 volume regulation. *JCell Physiol* 167: 60-71, 1996.
- 607 39. **Hamill OP.** Twenty odd years of stretch-sensitive channels. *Pflugers Arch* 453:
608 333-351, 2006.
- 609 40. **Hansma PK, Drake B, Marti O, Gould SA, and Prater CB.** The scanning
610 ion-conductance microscope. *Science* 243: 641-643, 1989.
- 611 41. **Hawes C, and Martin B.** Freeze-fracture deep-etch methods. *Methods Cell*
612 *Biol* 49: 33-43, 1995.
- 613 42. **Haydon PG, Lartius R, Parpura V, and Marchese-Ragona SP.** Membrane
614 deformation of living glial cells using atomic force microscopy. *JMicrosc* 182:
615 114-120, 1996.
- 616 43. **Hisatsune C, and Mikoshiba K.** Novel compartment implicated in calcium
617 signaling--is it an "induced coupling domain"? *SciSTKE* 2005: e53, 2005.
- 618 44. **Hochmuth RM.** Micropipette aspiration of living cells. *JBiomech* 33: 15-22,
619 2000.

- 620 45. **Hoffmann EK.** Cell swelling and volume regulation. *CanJPhysiol Pharmacol* 70
621 Suppl: S310-S313, 1992.
- 622 46. **Horber JK, and Miles MJ.** Scanning probe evolution in biology. *Science* 302:
623 1002-1005, 2003.
- 624 47. **Hur EM, and Kim KT.** G protein-coupled receptor signalling and cross-talk:
625 achieving rapidity and specificity. *Cell Signal* 14: 397-405, 2002.
- 626 48. **Inoue R, Jian Z, and Kawarabayashi Y.** Mechanosensitive TRP channels in
627 cardiovascular pathophysiology. *PharmacolTher* 123: 371-385, 2009.
- 628 49. **Isenberg G, Kazanski V, Kondratev D, Gallitelli MF, Kiseleva I, and**
629 **Kamkin A.** Differential effects of stretch and compression on membrane
630 currents and $[Na^+]_c$ in ventricular myocytes. *ProgBiophysMolBiol* 82: 43-56,
631 2003.
- 632 50. **Jacot JG, Dianis S, Schnall J, and Wong JY.** A simple microindentation
633 technique for mapping the microscale compliance of soft hydrated materials
634 and tissues. *JBiomedMaterResA* 79: 485-494, 2006.
- 635 51. **Janmey PA, Winer JP, Murray ME, and Wen Q.** The hard life of soft cells.
636 *Cell MotilCytoskeleton* 66: 597-605, 2009.
- 637 52. **Karoutsos V.** Scanning probe microscopy: instrumentation and applications
638 on thin films and magnetic multilayers. *JNanosciNanotechnol* 9: 6783-6798,
639 2009.
- 640 53. **Kawahara K, Onodera M, and Fukuda Y.** A simple method for continuous
641 measurement of cell height during a volume change in a single A6 cell.
642 *JpnJPhysiol* 44: 411-419, 1994.
- 643 54. **Khayutin VM, Lukoshkova EV, Rogoza AN, and Nikolsky VP.** Negative
644 feedbacks in the pathogenesis of primary arterial hypertension:
645 mechanosensitivity of the endothelium. *Blood Press* 4: 70-76, 1995.

- 646 55. **Klenerman D, and Korchev Y.** Potential biomedical applications of the
647 scanned nanopipette. *Nanomedicine(Lond)* 1: 107-114, 2006.
- 648 56. **Kohl P, Camelliti P, Burton FL, and Smith GL.** Electrical coupling of
649 fibroblasts and myocytes: relevance for cardiac propagation. *JElectrocardiol*
650 38: 45-50, 2005.
- 651 57. **Korchev YE, Bashford CL, Milovanovic M, Vodyanoy I, and Lab MJ.**
652 Scanning ion conductance microscopy of living cells. *BiophysJ* 73: 653-658,
653 1997.
- 654 58. **Korchev YE, Gorelik J, Lab MJ, Sviderskaya EV, Johnston CL, Coombes**
655 **CR, Vodyanoy I, and Edwards CR.** Cell volume measurement using
656 scanning ion conductance microscopy. *BiophysJ* 78: 451-457, 2000.
- 657 59. **Korchev YE, Milovanovic M, Bashford CL, Bennett DC, Sviderskaya EV,**
658 **Vodyanoy I, and Lab MJ.** Specialized scanning ion-conductance microscope
659 for imaging of living cells. *JMicrosc* 188: 17-23, 1997.
- 660 60. **Korchev YE, Negulyaev YA, Edwards CR, Vodyanoy I, and Lab MJ.**
661 Functional localization of single active ion channels on the surface of a living
662 cell. *NatCell Biol* 2: 616-619, 2000.
- 663 61. **Korchev YE, Raval M, Lab MJ, Gorelik J, Edwards CR, Rayment T, and**
664 **Klenerman D.** Hybrid scanning ion conductance and scanning near-field
665 optical microscopy for the study of living cells. *BiophysJ* 78: 2675-2679, 2000.
- 666 62. **Kordylewski L, Karrison T, and Page E.** P-face particle density of freeze-
667 fractured vertebrate cardiac plasma membrane. *AmJPhysiol* 245: H992-H997,
668 1983.
- 669 63. **Kurachi Y, and Ishii M.** Cell signal control of the G protein-gated potassium
670 channel and its subcellular localization. *JPhysiol* 554: 285-294, 2004.

- 671 64. **Kuznetsova TG, Starodubtseva MN, Yegorenkov NI, Chizhik SA, and**
672 **Zhdanov RI.** Atomic force microscopy probing of cell elasticity. *Micron* 38:
673 824-833, 2007.
- 674 65. **Lab M.** Scanning Ion Conductance Microscopy for Imaging and
675 Mechanosensitive Activation of Selected Areas of Live Cells. *Mechanosensitivity*
676 *of the Heart* 3: 6, 2012.
- 677 66. **Lab MJ.** Mechanically Mediated Crosstalk in Heart. 2005.
- 678 67. **Laforge FO, Carpino J, Rotenberg SA, and Mirkin MV.** Electrochemical
679 attosyringe. *ProcNatlAcadSciUSA* 104: 11895-11900, 2007.
- 680 68. **Lekka M, Fornal M, Pyka-Fosciak G, Lebed K, Wizner B, Grodzicki T,**
681 **and Styczen J.** Erythrocyte stiffness probed using atomic force microscope.
682 *Biorheology* 42: 307-317, 2005.
- 683 69. **Lesniewska E, Giocondi MC, Vie V, Finot E, Goudonnet JP, and Le GC.**
684 Atomic force microscopy of renal cells: limits and prospects. *Kidney IntSuppl*
685 65: S42-S48, 1998.
- 686 70. **Liu Y, Feng J, Shi L, Niu R, Sun Q, Liu H, Li J, Guo J, Zhu J, and Han D.**
687 In situ mechanical analysis of cardiomyocytes at nano scales. *Nanoscale* 4:
688 99-102, 2012.
- 689 71. **Ludwig T, Kirmse R, Poole K, and Schwarz US.** Probing cellular
690 microenvironments and tissue remodeling by atomic force microscopy.
691 *Pflugers Arch* 456: 29-49, 2008.
- 692 72. **Lyon AR, Macleod KT, Zhang Y, Garcia E, Kanda GK, Lab MJ, Korchev**
693 **YE, Harding SE, and Gorelik J.** Loss of T-tubules and other changes to
694 surface topography in ventricular myocytes from failing human and rat heart.
695 *ProcNatlAcadSciUSA* 106: 6854-6859, 2009.

- 696 73. **Mader A, Gruber K, Castelli R, Hermann BA, Seeberger PH, Radler JO,**
697 **and Leisner M.** Discrimination of *Escherichia coli* strains using glycan
698 cantilever array sensors. *NanoLett* 12: 420-423, 2012.
- 699 74. **Manley S, Gillette JM, Patterson GH, Shroff H, Hess HF, Betzig E, and**
700 **Lippincott-Schwartz J.** High-density mapping of single-molecule trajectories
701 with photoactivated localization microscopy. *NatMethods* 5: 155-157, 2008.
- 702 75. **McManus ML, and Strange K.** Acute volume regulation of brain cells in
703 response to hypertonic challenge. *Anesthesiology* 78: 1132-1137, 1993.
- 704 76. **Meyer HW, and Richter W.** Freeze-fracture studies on lipids and
705 membranes. *Micron* 32: 615-644, 2001.
- 706 77. **Miragoli M, Lab MJ, Sikkel M, Lyon AR, and Gorelik J.** Structural
707 Remodeling in Cardiomyocytes from Infarcted Hearts Potentiates Cellular
708 Mechano Arrhythmic response to Nanoscale Sarcolemmal Perturbation.
709 *Circulation Meeting abstract* 124: 2011.
- 710 78. **Mitsuoka K.** Obtaining high-resolution images of biological macromolecules
711 by using a cryo-electron microscope with a liquid-helium cooled stage. *Micron*
712 42: 100-106, 2011.
- 713 79. **Moe PC, Blount P, and Kung C.** Functional and structural conservation in the
714 mechanosensitive channel MscL implicates elements crucial for
715 mechanosensation. *MolMicrobiol* 28: 583-592, 1998.
- 716 80. **Morris CE.** Mechanosensitive ion channels. *JMembrBiol* 113: 93-107, 1990.
- 717 81. **Muller DJ, Helenius J, Alsteens D, and Dufrene YF.** Force probing surfaces
718 of living cells to molecular resolution. *Nature chemical biology* 5: 383-390,
719 2009.
- 720 82. **Muraki K, Shigekawa M, and Imaizumi Y.** A New Insight into the Function
721 of TRPV2 in Circulatory Organs. 2007.

- 722 83. **Myhra S.** A review of enabling technologies based on scanning probe
723 microscopy relevant to bioanalysis. *BiosensBioelectron* 19: 1345-1354, 2004.
- 724 84. **Nakahari T, Murakami M, Yoshida H, Miyamoto M, Sohma Y, and Imai**
725 **Y.** Decrease in rat submandibular acinar cell volume during ACh stimulation.
726 *AmJPhysiol* 258: G878-G886, 1990.
- 727 85. **Nikolaev VO, Moshkov A, Lyon AR, Miragoli M, Novak P, Paur H, Lohse**
728 **MJ, Korchev YE, Harding SE, and Gorelik J.** Beta2-adrenergic receptor
729 redistribution in heart failure changes cAMP compartmentation. *Science* 327:
730 1653-1657, 2010.
- 731 86. **Novak P, Li C, Shevchuk AI, Stepanyan R, Caldwell M, Hughes S, Smart**
732 **TG, Gorelik J, Ostanin VP, Lab MJ, Moss GW, Frolenkov GI, Klenerman**
733 **D, and Korchev YE.** Nanoscale live-cell imaging using hopping probe ion
734 conductance microscopy. *NatMethods* 6: 279-281, 2009.
- 735 87. **Oberleithner H.** Nanophysiology: fact or fiction? *Pflugers Archiv : European*
736 *journal of physiology* 456: 1-2, 2008.
- 737 88. **Orchard C, and Brette F.** t-Tubules and sarcoplasmic reticulum function in
738 cardiac ventricular myocytes. *CardiovascRes* 77: 237-244, 2008.
- 739 89. **Papp S, Dziak E, Michalak M, and Opas M.** Is all of the endoplasmic
740 reticulum created equal? The effects of the heterogeneous distribution of
741 endoplasmic reticulum Ca²⁺-handling proteins. *JCell Biol* 160: 475-479, 2003.
- 742 90. **Peyton SR, Ghajar CM, Khatiwala CB, and Putnam AJ.** The emergence of
743 ECM mechanics and cytoskeletal tension as important regulators of cell
744 function. *Cell BiochemBiophys* 47: 300-320, 2007.
- 745 91. **Piper JD, Clarke RW, Korchev YE, Ying L, and Klenerman D.** A renewable
746 nanosensor based on a glass nanopipette. *JAmChemSoc* 128: 16462-16463,
747 2006.

- 748 92. **Poggi MA, Gadsby ED, Bottomley LA, King WP, Oroudjev E, and**
749 **Hansma H.** Scanning probe microscopy. *AnalChem* 76: 3429-3443, 2004.
- 750 93. **Potter CM, Schobesberger S, Lundberg MH, Weinberg PD, Mitchell JA,**
751 **and Gorelik J.** Shape and compliance of endothelial cells after shear stress in
752 vitro or from different aortic regions: scanning ion conductance microscopy
753 study. *PLoSOne* 7: e31228, 2012.
- 754 94. **Quist AP, Bergman AA, Reimann CT, Oscarsson SO, and Sundqvist BU.**
755 Imaging of single antigens, antibodies, and specific immunocomplex formation
756 by scanning force microscopy. *Scanning Microsc* 9: 395-400, 1995.
- 757 95. **Ramachandran S, Teran AF, and Lal R.** Potential role of atomic force
758 microscopy in systems biology. *WileyInterdiscipRevSystBiolMed* 3: 702-716,
759 2011.
- 760 96. **Rheinlaender J, Geisse NA, Proksch R, and Schaffer TE.** Comparison of
761 scanning ion conductance microscopy with atomic force microscopy for cell
762 imaging. *Langmuir* 27: 697-704, 2011.
- 763 97. **Rheinlaender J, and Schaffer TE.** Image formation, resolution, and height
764 measurement in scanning ion conductance microscopy. *J Appl Phys* 105: 9,
765 2009
- 766
- 767 98. **Rodolfa KT, Bruckbauer A, Zhou D, Korchev YE, and Klenerman D.** Two-
768 component graded deposition of biomolecules with a double-barreled
769 nanopipette. *AngewChemIntEd Engl* 44: 6854-6859, 2005.
- 770 99. **Rotsch C, Braet F, Wisse E, and Radmacher M.** AFM imaging and elasticity
771 measurements on living rat liver macrophages. *Cell BiolInt* 21: 685-696, 1997.
- 772 100. **Sanchez D, Johnson N, Li C, Novak P, Rheinlaender J, Zhang Y, Anand**
773 **U, Anand P, Gorelik J, Frolenkov GI, Benham C, Lab M, Ostanin VP,**

- 774 **Schaffer TE, Klenerman D, and Korchev YE.** Noncontact measurement of
775 the local mechanical properties of living cells using pressure applied via a
776 pipette. *BiophysJ* 95: 3017-3027, 2008.
- 777 101. **Schermelleh L, Heintzmann R, and Leonhardt H.** A guide to super-
778 resolution fluorescence microscopy. *The Journal of cell biology* 190: 165-175,
779 2010.
- 780 102. **Scott JD.** A-kinase-anchoring proteins and cytoskeletal signalling events.
781 *BiochemSocTrans* 31: 87-89, 2003.
- 782 103. **Sen S, Subramanian S, and Discher DE.** Indentation and adhesive probing
783 of a cell membrane with AFM: theoretical model and experiments. *BiophysJ*
784 89: 3203-3213, 2005.
- 785 104. **Shevchuk AI, Frolenkov GI, Sanchez D, James PS, Freedman N, Lab**
786 **MJ, Jones R, Klenerman D, and Korchev YE.** Imaging proteins in
787 membranes of living cells by high-resolution scanning ion conductance
788 microscopy. *AngewChemIntEd Engl* 45: 2212-2216, 2006.
- 789 105. **Shevchuk AI, Hobson P, Lab MJ, Klenerman D, Krauzewicz N, and**
790 **Korchev YE.** Endocytic pathways: combined scanning ion conductance and
791 surface confocal microscopy study. *Pflugers Arch* 456: 227-235, 2008.
- 792 106. **Shevchuk AI, Hobson P, Lab MJ, Klenerman D, Krauzewicz N, and**
793 **Korchev YE.** Imaging single virus particles on the surface of cell membranes
794 by high-resolution scanning surface confocal microscopy. *BiophysJ* 94: 4089-
795 4094, 2008.
- 796 107. **Shevchuk AI, Novak P, Takahashi Y, Clarke R, Miragoli M, Babakinejad**
797 **B, Gorelik J, Korchev YE, and Klenerman D.** Realizing the biological and
798 biomedical potential of nanoscale imaging using a pipette probe.
799 *Nanomedicine(Lond)* 6: 565-575, 2011.

- 800 108. **Stewart MP, Toyoda Y, Hyman AA, and Muller DJ.** Force probing cell
801 shape changes to molecular resolution. *Trends BiochemSci* 36: 444-450,
802 2011.
- 803 109. **Stolz M, Raiteri R, Daniels AU, VanLandingham MR, Baschong W, and**
804 **Aebi U.** Dynamic elastic modulus of porcine articular cartilage determined at
805 two different levels of tissue organization by indentation-type atomic force
806 microscopy. *BiophysJ* 86: 3269-3283, 2004.
- 807 110. **Sun HW, and Suo R.** [Investigation of enhancing effect for hydride
808 generation-atomic fluorescence of transition metal elements]. *GuangPuXueYu*
809 *GuangPuFenXi* 28: 2684-2690, 2008.
- 810 111. **Svoboda K, and Block SM.** Biological applications of optical forces.
811 *AnnuRevBiophysBiomolStruct* 23: 247-285, 1994.
- 812 112. **Takahashi Y, Shevchuk AI, Novak P, Zhang Y, Ebejer N, Macpherson**
813 **JV, Unwin PR, Pollard AJ, Roy D, Clifford CA, Shiku H, Matsue T,**
814 **Klenerman D, and Korchev YE.** Multifunctional nanoprobes for nanoscale
815 chemical imaging and localized chemical delivery at surfaces and interfaces.
816 *AngewChemIntEd Engl* 50: 9638-9642, 2011.
- 817 113. **te RJ, Katan AJ, Rankl C, Stahl SW, van Buul AM, Phang IY, Gomez-**
818 **Casado A, Schon P, Gerritsen JW, Cambi A, Rowan AE, Vancso GJ,**
819 **Jonkheijm P, Huskens J, Oosterkamp TH, Gaub H, Hinterdorfer P,**
820 **Figdor CG, and Speller S.** Interlaboratory round robin on cantilever
821 calibration for AFM force spectroscopy. *Ultramicroscopy* 111: 1659-1669,
822 2011.
- 823 114. **Tosolini G, Villanueva LG, Perez-Murano F, and Bausells J.** Fast on-wafer
824 electrical, mechanical, and electromechanical characterization of piezoresistive
825 cantilever force sensors. *RevSciInstrum* 83: 015002, 2012.

- 826 115. **Turner YT, Roberts CJ, and Davies MC.** Scanning probe microscopy in the
827 field of drug delivery. *AdvDrug DelivRev* 59: 1453-1473, 2007.
- 828 116. **van de Linde S, Loschberger A, Klein T, Heidebreder M, Wolter S,**
829 **Heilemann M, and Sauer M.** Direct stochastic optical reconstruction
830 microscopy with standard fluorescent probes. *Nature protocols* 6: 991-1009,
831 2011.
- 832 117. **Webb HK, Truong VK, Hasan J, Crawford RJ, and Ivanova EP.** Physico-
833 mechanical characterisation of cells using atomic force microscopy - Current
834 research and methodologies. *JMicrobiolMethods* 86: 131-139, 2011.
- 835 118. **White E.** Mechanosensitive channels: therapeutic targets in the myocardium?
836 *CurrPharmDes* 12: 3645-3663, 2006.
- 837 119. **Willig KI, Kellner RR, Medda R, Hein B, Jakobs S, and Hell SW.**
838 Nanoscale resolution in GFP-based microscopy. *NatMethods* 3: 721-723, 2006.
- 839 120. **Wozniak M, Keefer JR, Saunders C, and Limbird LE.** Differential targeting
840 and retention of G protein-coupled receptors in polarized epithelial cells.
841 *JReceptSignalTransductRes* 17: 373-383, 1997.
- 842 121. **Xu LP, Liu Y, and Zhang X.** Interfacial self-assembly of amino acids and
843 peptides: scanning tunneling microscopy investigation. *Nanoscale* 3: 4901-
844 4915, 2011.
- 845 122. **Ying L, Bruckbauer A, Zhou D, Gorelik J, Shevchuk A, Lab M, Korchev**
846 **Y, and Klenerman D.** The scanned nanopipette: a new tool for high
847 resolution bioimaging and controlled deposition of biomolecules.
848 *PhysChemChemPhys* 7: 2859-2866, 2005.
- 849 123. **You HX, Lau JM, Zhang S, and Yu L.** Atomic force microscopy imaging of
850 living cells: a preliminary study of the disruptive effect of the cantilever tip on
851 cell morphology. *Ultramicroscopy* 82: 297-305, 2000.

- 852 124. **Yu H, Yang T, Chen Y, Xu P, Lee DW, and Li X.** Chemo-mechanical joint
853 detection with both dynamic and static microcantilevers for interhomologue
854 molecular identification. *AnalChem* 84: 6679-6685, 2012.
- 855 125. **Zhang Y, Gorelik J, Sanchez D, Shevchuk A, Lab M, Vodyanoy I,**
856 **Klenerman D, Edwards C, and Korchev Y.** Scanning ion conductance
857 microscopy reveals how a functional renal epithelial monolayer maintains its
858 integrity. *Kidney Int* 68: 1071-1077, 2005.
- 859 126. **Zhu J, Sabharwal T, Kalyanasundaram A, Guo L, and Wang G.**
860 Topographic mapping and compression elasticity analysis of skinned cardiac
861 muscle fibers in vitro with atomic force microscopy and nanoindentation.
862 *JBiomech* 42: 2143-2150, 2009.
- 863 127. **Zhu Q, Tekola P, Baak JP, and Belien JA.** Measurement by confocal laser
864 scanning microscopy of the volume of epidermal nuclei in thick skin sections.
865 *AnalQuantCytolHistol* 16: 145-152, 1994.
- 866
- 867
- 868

869 **Figure Legends**

870

871 **Figure 1. Schematic diagram of Scanning Ion Conductance Microscope**

872 **(SICM).** The electrolyte-filled scanning nanopipette is mounted on a piezo
873 translation platform. It also contains an Ag/AgCl electrode connected to an ion
874 current detector/amplifier above. The input to this detector is an ion current signal
875 from the bath (left hand side vertical line). The amplifier's output drives a feedback
876 control amplifier (right hand side vertical line) to control the pipette's piezo, which
877 provides a Z only directional movement (up and down). It also provides a drive to
878 the nanopositioning stage (bottom) but raster scanning in two directions (X Y). An
879 optical system under the nanopositioning stage focuses a laser to a confocal volume
880 near the pipette's tip, and also provides the required detection system.

881

882 **Figure 2. Functional localization of β AR-induced cAMP signaling and the**
883 **principle of the combined nanoscale SICM-FRET approach. A)** SICM surface

884 image indicating the positioning of the pipette, and diagramming isoprenaline (ISO)
885 application. **B)** Scheme of receptor activity measured by monitoring the production
886 of cAMP by Epac2-camps, a FRET-based cAMP sensor that changes its conformation
887 and fluorescence properties upon activation—i.e.cAMP binding. YFP and CFP, yellow
888 and cyan fluorescent proteins, respectively. **C)** Healthy cardiomyocyte with a well-
889 defined surface topography showing its regular surface structure. Z grooves
890 separating crests provide a scalloped surface, with T tubules visible in the grooves –
891 good Z groove index – see text. **D)** FRET ratio on application of ISO to T-tubule or
892 crest in healthy myocardium. A response was only recorded in the T-tubular regions
893 suggesting the β_2 AR is preferentially localized here. **E)** Cardiomyocyte from a rat
894 with myocardial failure, showing a disrupted surface topography. There is no clear

895 relation between T tubules and Z grooves - poor Z groove index. **F)** ISO application
896 produces cAMP signals both in T-tubules and crest suggesting the loss of cAMP
897 compartmentation in heart failure.

898

899 **Figure 3. L type calcium channel (LTCC) distribution in the cardiomyocyte**
900 **membrane: mapping of ion channels by the “smart” patch-clamp**
901 **technique. A)** Adult rat cardiomyocyte and micropipette as seen by optical
902 microscope. **B)** Diagram of smart patch circuitry with vertical pipette. **C)**
903 Cardiomyocyte topography showing the regular Z grooves and crests (scalloped
904 surface) with T-tubules **D)** Schematic of myocyte cross-section with probe
905 positioning in sarcomere units (Z-groove, T-tubule opening and scallop crest).
906 Probabilities of forming a $G\Omega$ seal as a function of surface position are shown in
907 parenthesis. **E)** Cell-attached Ba^{2+} currents at 0 mV showing several current traces
908 and ensemble average of 12 traces showing typical LTCC current kinetics. **F)**
909 Diagrammatic representation of statistical distribution of LTCCs with the highest
910 density near the T-tubule opening. Modified from (35) with permission.

911

912 **Figure 4. Vertical (Z) Deflection and Signal Detection. (A).** Diagram of
913 vertical displacement (contraction) measure and illumination with calcium
914 detection. The SICM pipette hovers above the myocyte. Its contraction is
915 represented by the relaxed myocyte (grey dotted outline) contracting inwards and
916 downwards (indicated by diagonal dashed arrows) to the contracted state of the
917 myocyte (solid outline). This contraction displaces the horizontal platform up and
918 down (Z deflection). Confocal illumination is from below, focussing on a confocal
919 volume beneath the myocyte membrane (small red rectangle). (B). Traces of
920 digitised Z deflection (left ordinate - contraction) is in black, with the calcium signal

921 in red (right ordinate). (C) Cardiomyocyte with diagrammed pipette applying
922 pressure in system with similar setup to (A). Pressure source ejects fluid from
923 pipette tip to indent cardiomyocyte membrane surface. (D) Subthreshold pressure
924 stimulation (left block arrow) produces a small indentation of about 0.5 μm (upward
925 deflection in height), whereas a higher threshold pressure (right block arrow) not
926 only produces a larger indentation, but elicits a contraction (sharpish upward
927 deflection

928

929 **Figure 5 Summary Diagram of overall functionality of the Scanning Ion**
930 **Conductance Microscope (SICM).** The pipette can function as various probes
931 (input to central SICM sphere from below.) The spokes radiating out from the SICM
932 sphere reach towards other spheres, which indicate the range of functionality. The
933 spheres on the left sub-serve its original and basic function as a microscope. It can
934 image large molecules through to a whole cell. The spheres on the right motion the
935 SICM's diverse hybrid function – the top two spheres, signal and
936 electrophysiological surface location (ion channels, receptors), and the bottom two
937 – mechanical.

938

939 **Table Legend**

940 **Table 1. Resolutions of microscopy techniques.** Abbreviations - nm =
941 nanometer; SICM = Scanning Ion Conductance Microscope; SEM = Scanning
942 Electron Microscope; TEM = Transmission Electron Microscope; AFM = Atomic Force
943 Microscope. ***Not ideal for cell surfaces**

Figure 1

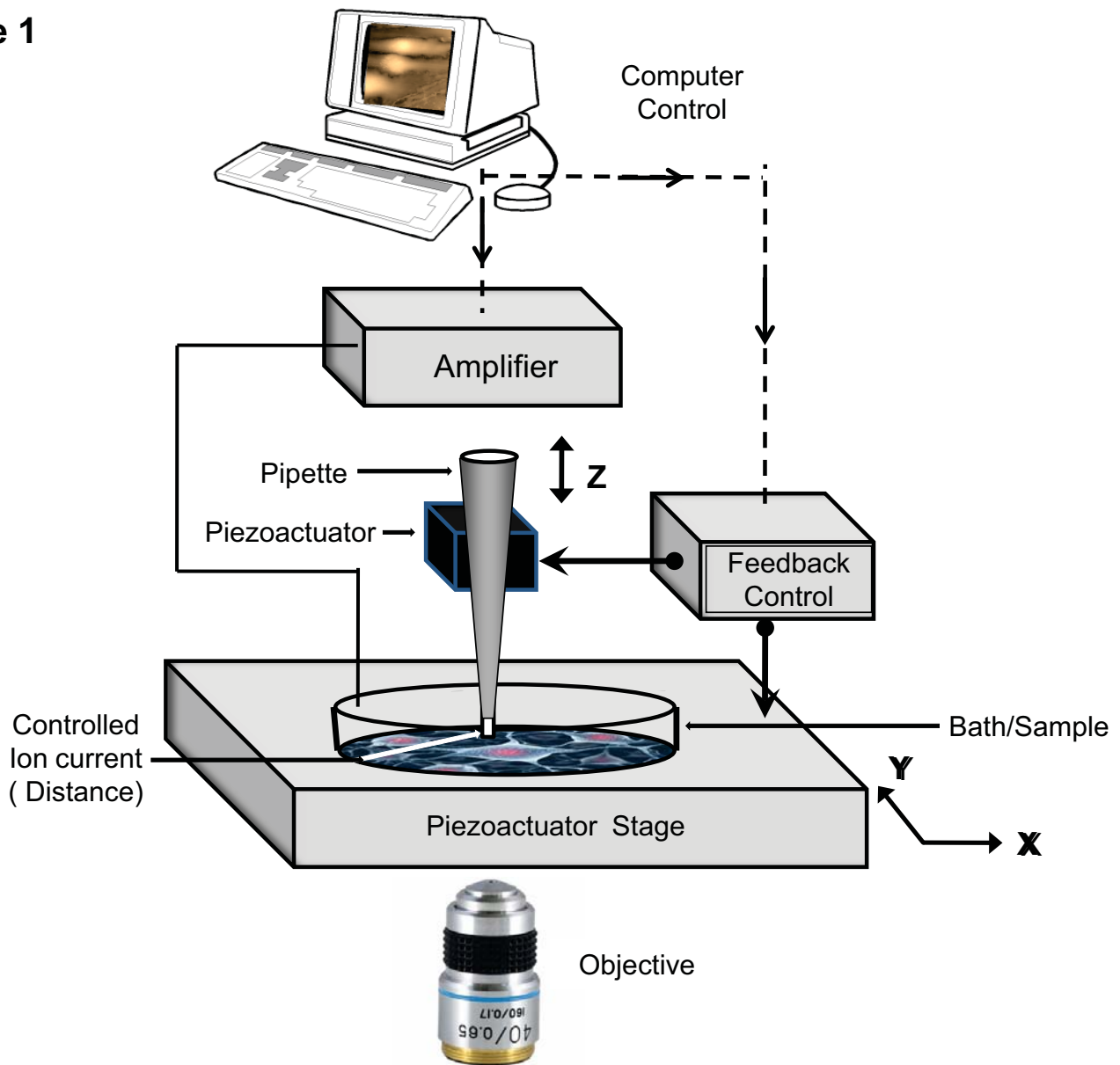


Figure 2

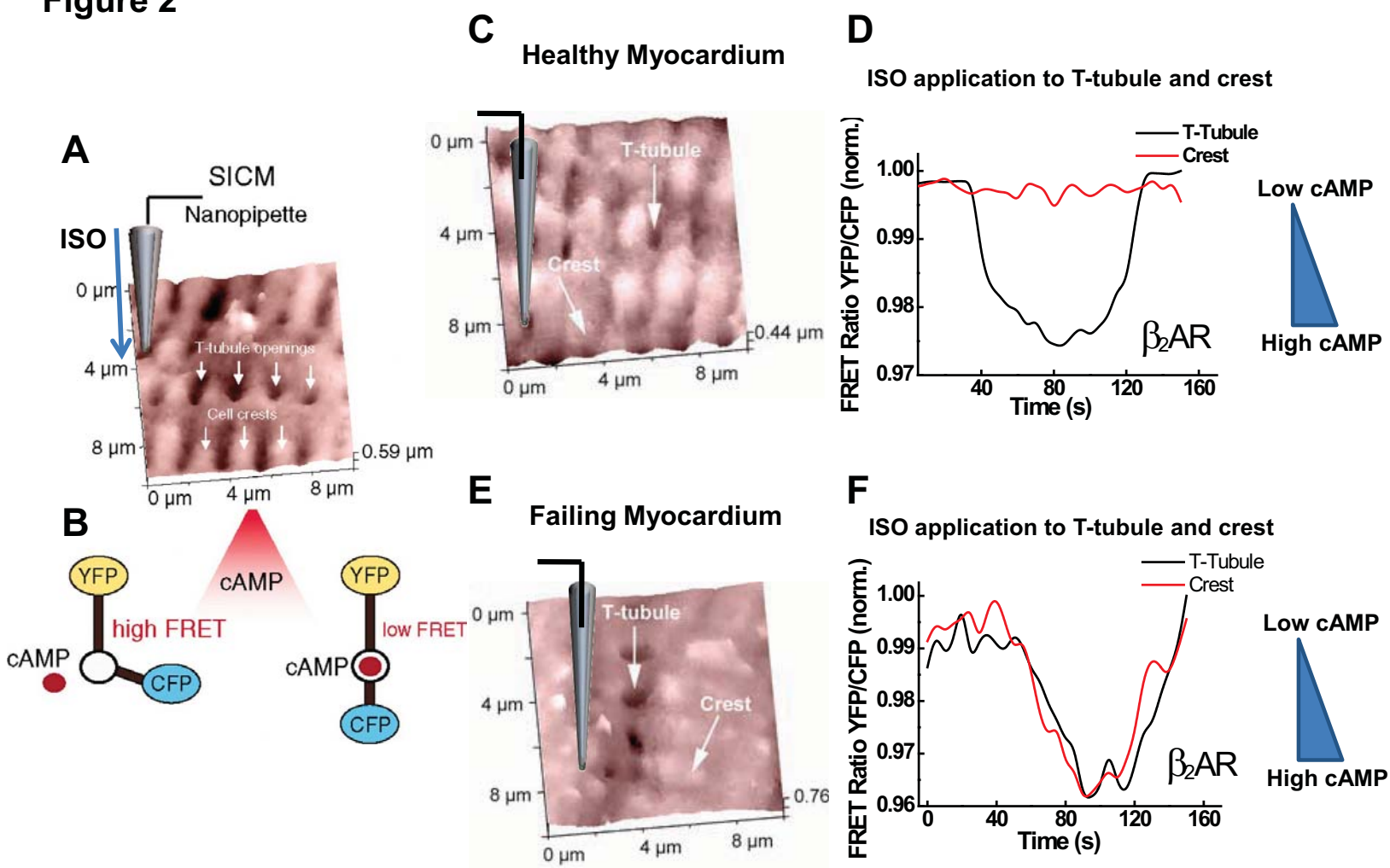


Figure 3

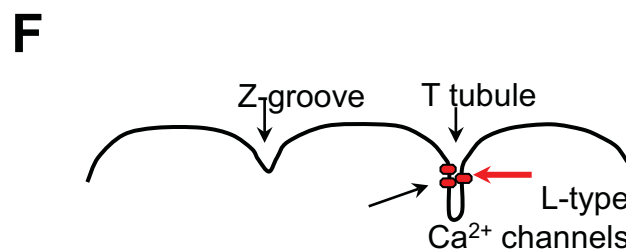
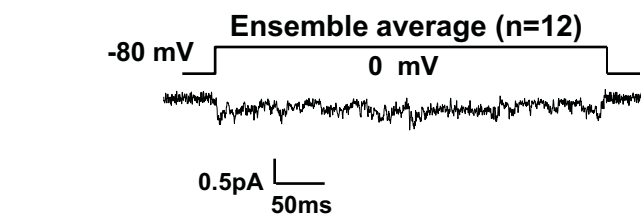
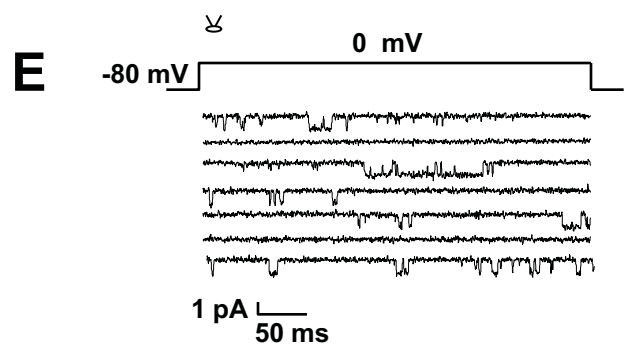
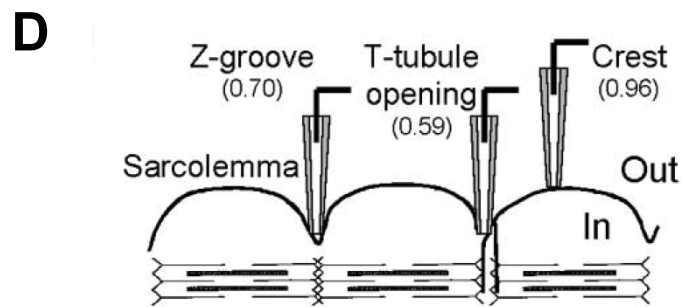
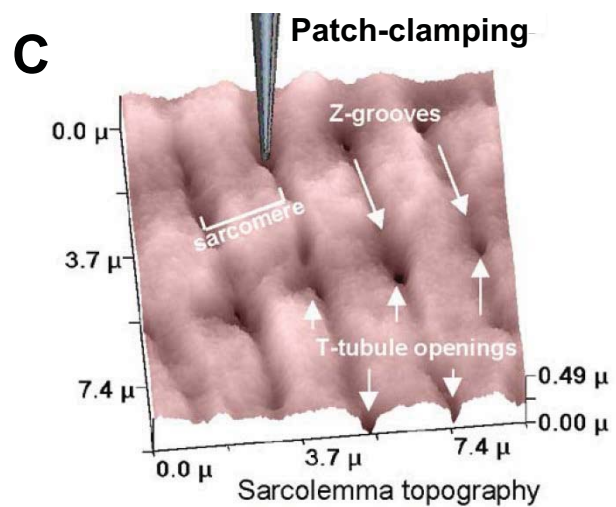
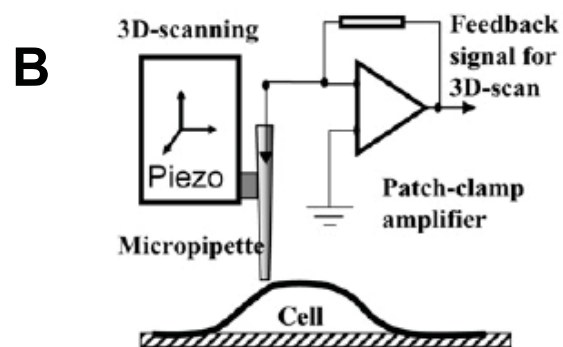
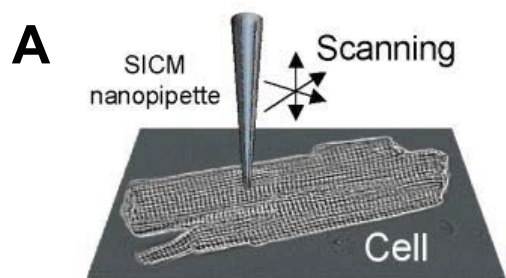


Figure 4

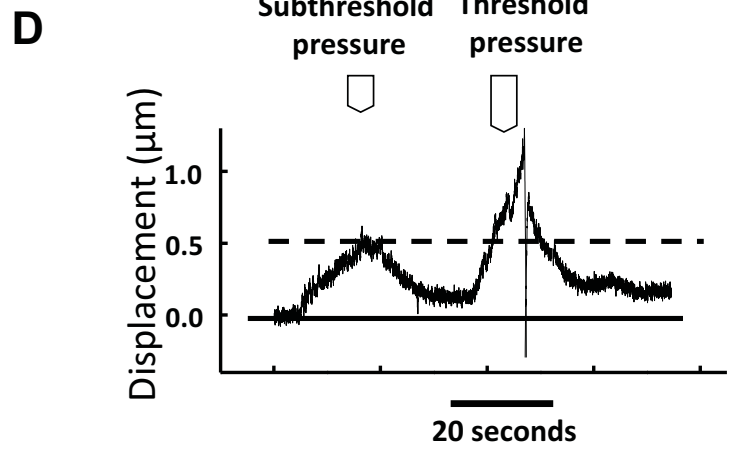
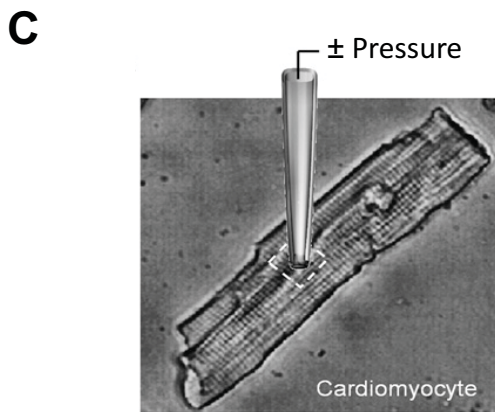
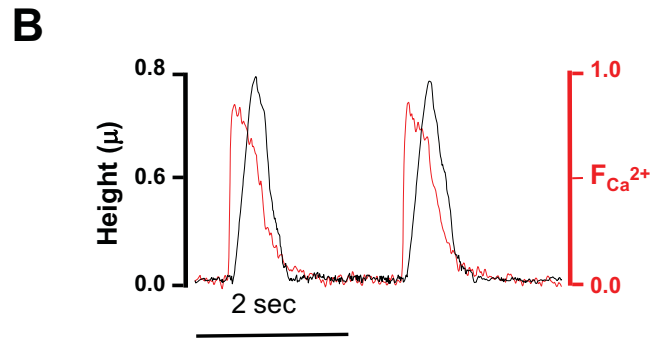
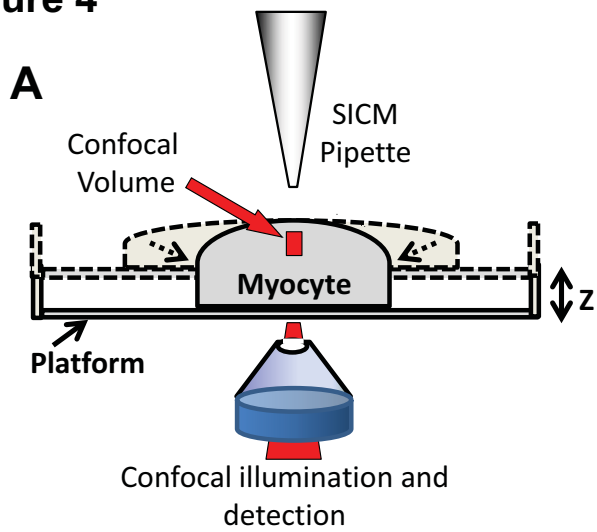


Figure 5

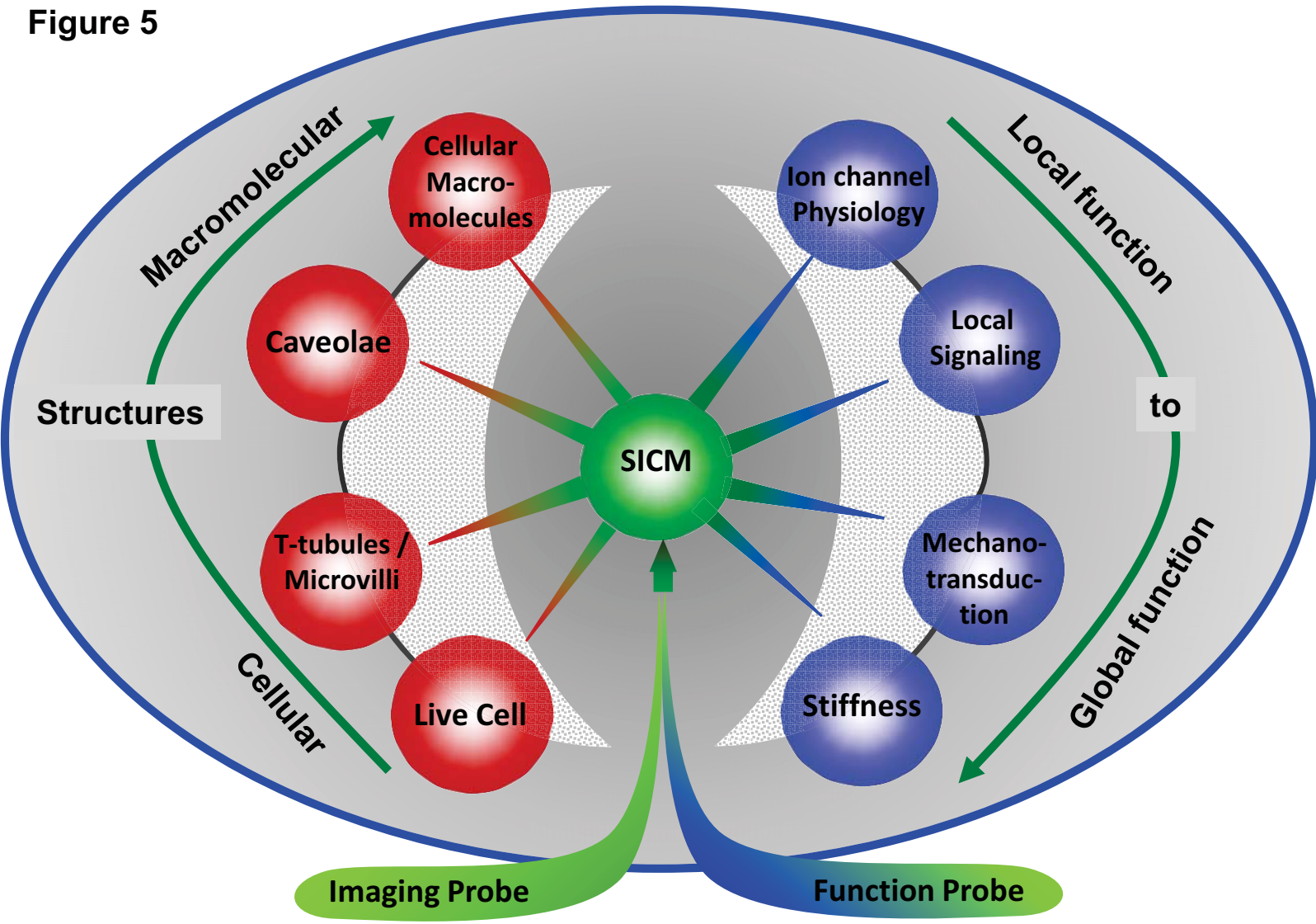


Table 1

Approx. Resolution (nm)	Microscope System	Principle of Operation	Sample preparation
~200 nm ~5-100 nm	Optical -Standard (116) Optical - Advanced (101)	Light- wavelength limited* Below light's wavelength*	Stained or unstained in liquid or air
~5- 200 nm	SICM (57, 104, 106)	Ion conductance via nanopipette.	In Ion Conducting Solution
0.5 - 10 nm	Electron - SEM (41, 76) Electron -TEM (18)	Electron beam Impede electrons	Electron conductive sample, vacuum Metal staining, vacuum
~10-50nm	AFM for live cells (81)	Force via sharp probe	In liquid or air